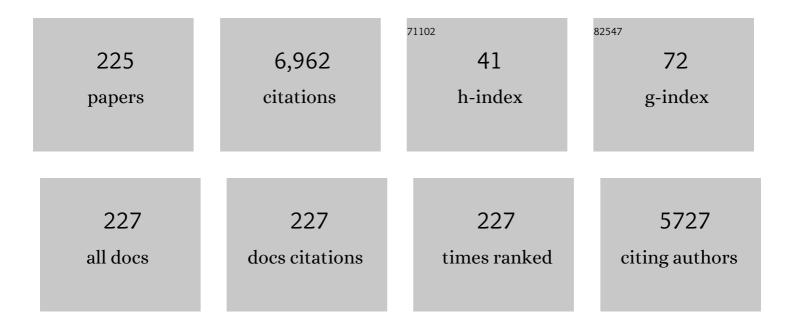
List of Publications by Year in descending order

Source: https://exaly.com/author-pdf/1388064/publications.pdf Version: 2024-02-01



IED-REN YANC

#	Article	IF	CITATIONS
1	Hierarchical nanotwins in Fe27Co24Ni23Cr26 high-entropy alloy subjected to high strain-rate Hopkinson bar deformation. Materials Characterization, 2022, 185, 111737.	4.4	8
2	Verification of the ability of Cu to dissolve in BCC δ in a δ-γ Solid Solution above 1200 °C and boosting δ nano-hardness in Cu-containing PHSS. Scripta Materialia, 2022, 211, 114505.	5.2	5
3	HR-STEM investigation of atomic lattice defects in different types of Î∙ precipitates in creep-age forming Al–Zn–Mg–Cu aluminium alloy. Materials Science & Engineering A: Structural Materials: Properties, Microstructure and Processing, 2021, 815, 141213.	5.6	22
4	Electron work function: an indicative parameter towards a novel material design methodology. Scientific Reports, 2021, 11, 11565.	3.3	17
5	Microstructural Characterization and Mechanical Properties of Duplex and Super Austenitic Stainless Steels under Dynamic Impact Deformation. Journal of Materials Engineering and Performance, 2021, 30, 8169.	2.5	2
6	Investigation on the ballistic induced nanotwinning in the Mn-free Fe27Co24Ni23Cr26 high entropy alloy plate. Materials Chemistry and Physics, 2021, 270, 124707.	4.0	13
7	Microstructural variation in fatigued interphase arrayed nano-precipitated Ti-microalloyed steel. Journal of Materials Research and Technology, 2021, 15, 2393-2404.	5.8	2
8	A novel technique for developing a dual-phase steel with a lower strength difference between ferrite and martensite. Materials Today Communications, 2020, 23, 100895.	1.9	11
9	Investigation of nanotwins in the bimodal-structured Fe22Co22Ni20Cr22Mn14 alloy subjected to high-strain-rate deformation at cryogenic temperatures. Materials Characterization, 2020, 170, 110667.	4.4	11
10	Microstructure Characterization of Massive Ferrite in Laser-Weldments of Interstitial-Free Steels. Metals, 2020, 10, 898.	2.3	3
11	Dielectric properties and reliability enhancement of atomic layer deposited thin films by <i>in situ</i> atomic layer substrate biasing. Journal of Materials Chemistry C, 2020, 8, 13025-13032.	5.5	4
12	Large Delta T Thermal Cycling Induced Stress Accelerates Equilibrium and Transformation in Super DSS. Crystals, 2020, 10, 962.	2.2	3
13	Characteristics of Flakes Stacked Cr2N with Many Domains in Super Duplex Stainless Steel. Crystals, 2020, 10, 965.	2.2	3
14	Atomic-resolution energy dispersive X-ray spectroscopy mapping of Ε precipitates in an Al-Mg-Zn-Cu alloy. Materials Characterization, 2020, 166, 110448.	4.4	12
15	Microstrain and boundary misorientation evolution for recrystallized super DSS after deformation. Materials Chemistry and Physics, 2020, 246, 122815.	4.0	12
16	Molybdenum alloying in high-performance flat-rolled steel grades. Advances in Manufacturing, 2020, 8, 15-34.	6.1	15
17	Metallurgical Effects of Niobium in Dual Phase Steel. Metals, 2020, 10, 504.	2.3	11
18	Low-Temperature Physical Adsorption for the Nucleation of Sub-10 nm Al2O3 Gate Stack on Top-Gated WS2 Transistors. ACS Applied Electronic Materials, 2020, 2, 1289-1294.	4.3	3

#	Article	IF	CITATIONS
19	CVD growth of large-area InS atomic layers and device applications. Nanoscale, 2020, 12, 9366-9374.	5.6	9
20	Twin relationship in between the variant-pair of η precipitates in the Al-Zn-Mg-Cu aluminium alloy. MATEC Web of Conferences, 2020, 326, 01002.	0.2	0
21	Characterization of nano-sized precipitation and dislocations and the correlation with mechanical properties of a low alloy TRIP-aided steel. Materials Science & Engineering A: Structural Materials: Properties, Microstructure and Processing, 2019, 763, 138149.	5.6	15
22	Thermal cycling induced stress–assisted sigma phase formation in super duplex stainless steel. Materials and Design, 2019, 182, 108003.	7.0	10
23	In-situ transmission electron microscopy investigation of compressive deformation in interphase-precipitatedÂcarbide-strengthened α-iron single-crystal nanopillars. Materials Science & Engineering A: Structural Materials: Properties, Microstructure and Processing, 2019, 746, 406-415.	5.6	7
24	Microstructure characterization and strengthening behavior of dual precipitation particles in Cu Ti microalloyed dual-phase steels. Materials and Design, 2019, 166, 107613.	7.0	13
25	Understanding Mechanical Properties of Nano-Grained Bainitic Steels from Multiscale Structural Analysis. Metals, 2019, 9, 426.	2.3	8
26	An atomic scale structural investigation of nanometre-sized ηÂprecipitates in the 7050 aluminium alloy. Acta Materialia, 2019, 174, 351-368.	7.9	110
27	Microstructure and mechanical behaviors of GPa-grade TRIP steels enabled by hot-rolling processes. Materials Science & Engineering A: Structural Materials: Properties, Microstructure and Processing, 2019, 761, 138005.	5.6	22
28	Microstructural mechanisms controlling the mechanical behaviour of ultrafine grained martensite/austenite microstructures in a metastable stainless steel. Materials and Design, 2019, 181, 107922.	7.0	17
29	Intrinsic twin boundary of ÎMgZn2 precipitates in the AA7050 aluminium alloy. Procedia Manufacturing, 2019, 37, 201-206.	1.9	5
30	High-entropy CoCrFeMnNi alloy subjected to high-strain-rate compressive deformation. Materials Characterization, 2019, 147, 193-198.	4.4	43
31	Strain rate dependence on the evolution of microstructure and deformation mechanism during nanoscale deformation in low carbon-high Mn TWIP steel. Materials Science & Engineering A: Structural Materials: Properties, Microstructure and Processing, 2019, 742, 116-123.	5.6	28
32	The application of convergent beam electron diffraction (CBED) analysis on transformationâ€induced plasticity (TRIP) steels. Microscopy Research and Technique, 2019, 82, 4-11.	2.2	1
33	Transmission electron microscopy investigation of separated nucleation and in-situ nucleation in AA7050 aluminium alloy. Acta Materialia, 2018, 149, 377-387.	7.9	168
34	The effect of finish rolling temperature and tempering on the microstructure, mechanical properties and dislocation density of direct-quenched steel. Materials Characterization, 2018, 139, 1-10.	4.4	58
35	Phase quantification in low carbon Nb-Mo bearing steel by electron backscatter diffraction technique coupled with kernel average misorientation. Materials Characterization, 2018, 139, 49-58.	4.4	61
36	Fatigue behavior and microstructural characteristics of a duplex stainless steel weld metal under vibration-assisted welding. Materials Science & Engineering A: Structural Materials: Properties, Microstructure and Processing, 2018, 721, 319-327.	5.6	8

#	Article	IF	CITATIONS
37	Crystallographic examination of the interaction between texture evolution, mechanically induced martensitic transformation and twinning in nanostructured bainite. Journal of Alloys and Compounds, 2018, 752, 505-519.	5.5	19
38	Precipitation behavior in bimodal ferrite grains in a low carbon Ti-V-bearing steel. Scripta Materialia, 2018, 143, 103-107.	5.2	11
39	Evolution of resistive switching mechanism through H 2 O 2 sensing by using TaO x -based material in W/Al 2 O 3 /TaO x /TiN structure. Applied Surface Science, 2018, 433, 51-59.	6.1	27
40	Modeling of Precipitation Hardening during Coiling of Nb–Mo Steels. Metals, 2018, 8, 758.	2.3	6
41	Size effect and strain induced double twin by nanoindentation in DSS weld metal of vibration-assisted GTAW. Materials Chemistry and Physics, 2018, 219, 40-50.	4.0	6
42	Morphological evolution of GP zones and nanometer-sized precipitates in the AA2050 aluminium alloy. International Journal of Lightweight Materials and Manufacture, 2018, 1, 142-156.	2.1	14
43	Impact of Intercritical Annealing on Retained Austenite and Toughness of a 460 MPa Grade Multiphase Heavy Gauge Plate Steel. Steel Research International, 2018, 89, 1800006.	1.8	2
44	Cross-Point Resistive Switching Memory and Urea Sensing by Using Annealed GdO _x Film in IrO _x /GdO _x /W Structure for Biomedical Applications. Journal of the Electrochemical Society, 2017, 164, B127-B135.	2.9	19
45	Effect of Cr and Al additions on the development of interphase-precipitated carbides strengthened dual-phase Ti-bearing steels. Materials and Design, 2017, 119, 319-325.	7.0	27
46	Densification, microstructure evolution, and microwave dielectric properties of Mg 1-x Ca x ZrTa 2 O 8 ceramics. Journal of the European Ceramic Society, 2017, 37, 2825-2831.	5.7	23
47	Effect of Boron on the Strength and Toughness of Direct-Quenched Low-Carbon Niobium Bearing Ultra-High-Strength Martensitic Steel. Metallurgical and Materials Transactions A: Physical Metallurgy and Materials Science, 2017, 48, 5344-5356.	2.2	25
48	Effect of interpass temperature on the microstructure and mechanical properties of multi-pass weld metal in a 550-MPa-grade offshore engineering steel. Welding in the World, Le Soudage Dans Le Monde, 2017, 61, 1155-1168.	2.5	41
49	Influence of welding pass on microstructure and toughness in the reheated zone of multi-pass weld metal of 550 MPa offshore engineering steel. Materials Science & Engineering A: Structural Materials: Properties, Microstructure and Processing, 2017, 702, 196-205.	5.6	47
50	Microstructural evolutions of low carbon Nb/Mo-containing bainitic steels during high-temperature tempering. Materials Characterization, 2017, 131, 298-305.	4.4	46
51	Negative voltage modulated multi-level resistive switching by using a Cr/BaTiOx/TiN structure and quantum conductance through evidence of H2O2 sensing mechanism. Scientific Reports, 2017, 7, 4735.	3.3	42
52	A unified constitutive model for asymmetric tension and compression creep-ageing behaviour of naturally aged Al-Cu-Li alloy. International Journal of Plasticity, 2017, 89, 130-149.	8.8	100
53	Investigation of idiomorphic ferrite and allotriomorphic ferrite using electron backscatter diffraction technique. Materials Science and Technology, 2017, 33, 537-545.	1.6	5
54	Effects of interphase TiC precipitates on tensile properties and dislocation structures in a dual phase steel. Materials Characterization, 2017, 123, 153-158.	4.4	40

#	Article	IF	CITATIONS
55	Severe deformation of nanostructured bainitic steel. Procedia Engineering, 2017, 207, 1862-1867.	1.2	4
56	Highly Reliable Label-Free Detection of Urea/Glucose and Sensing Mechanism Using SiO2and CdSe-ZnS Nanoparticles in Electrolyte-Insulator-Semiconductor Structure. Journal of the Electrochemical Society, 2016, 163, B580-B587.	2.9	17
57	In-situ transmission electron microscopy investigation of the deformation behavior of spinodal nanostructured δ-ferrite in a duplex stainless steel. Scripta Materialia, 2016, 125, 44-48.	5.2	34
58	Detection of pH and Enzyme-Free H2O2 Sensing Mechanism by Using GdO x Membrane in Electrolyte-Insulator-Semiconductor Structure. Nanoscale Research Letters, 2016, 11, 434.	5.7	6
59	Investigation of the microstructure and toughness of 550â€MPa grade pipeline after the hot-bending process. Materials Science and Technology, 2016, 32, 664-674.	1.6	3
60	Microstructural characterization and strengthening behavior of nanometer sized carbides in Ti–Mo microalloyed steels during continuous cooling process. Materials Characterization, 2016, 114, 18-29.	4.4	40
61	Mechanical behavior and microstructural evolution of nanostructured bainite under high-strain rate deformation by Hopkinson bar. Scripta Materialia, 2016, 115, 46-51.	5.2	23
62	Investigation of photoluminescence dynamics in InGaN/GaN multiple quantum wells. Materials Letters, 2016, 173, 170-173.	2.6	6
63	Crystallographic analysis of lenticular martensite in Fe–1.0C–17Cr stainless steel by electron backscatter diffraction. Materials Characterization, 2016, 113, 17-25.	4.4	13
64	B22-P-09The misorientation change in lenticular martensite by Electron Backscattered Diffraction and Convergent Beam Kikuchi Line Diffraction Pattern. Microscopy (Oxford, England), 2015, 64, i107.1-i107.	1.5	0
65	B11-P-11The effect of aging on the phase transformation of AA7050 aluminum alloys. Microscopy (Oxford, England), 2015, 64, i83.2-i83.	1.5	0
66	Structure and electrical property changes of ZnO:Al films, prepared by radio frequency magnetron sputtering, by thermal annealing. Microscopy and Microanalysis, 2015, 21, 1797-1798.	0.4	0
67	Structure of Ru/Pt Nanocomposite Films Fabricated by Plasma-Enhanced Atomic Layer Depositions. Microscopy and Microanalysis, 2015, 21, 1931-1932.	0.4	0
68	B12-O-18Insight into the Deformation Behavior of Spinodal Nanostructured δ-Ferrite in a 2205 Duplex Stainless Steel. Microscopy (Oxford, England), 2015, 64, i27.2-i27.	1.5	0
69	Retarded phase transition by fluorine doping in Li-rich layered Li 1.2 Mn 0.54 Ni 0.13 Co 0.13 O 2 cathode material. Journal of Power Sources, 2015, 283, 162-170.	7.8	190
70	Microstructural characterization of Charpy-impact-tested nanostructured bainite. Materials Characterization, 2015, 107, 63-69.	4.4	37
71	Structural investigation of Ru/Pt nanocomposite films prepared by plasma-enhanced atomic layer depositions. Micron, 2015, 74, 8-14.	2.2	4
72	Improved resistive switching phenomena and mechanism using Cu-Al alloy in a new Cu:AlOx/TaOx/TiN structure. Journal of Alloys and Compounds, 2015, 637, 517-523.	5.5	35

#	Article	IF	CITATIONS
73	Tensile Response of Two Nanoscale Bainite Composite-Like Structures. Jom, 2015, 67, 2223-2235.	1.9	48
74	Synergistic effect of austenitizing temperature and hot plastic deformation strain on the precipitation behavior in novel HSLA steel. Materials Science & Engineering A: Structural Materials: Properties, Microstructure and Processing, 2015, 639, 145-154.	5.6	16
75	Ultralow threading dislocation density in GaN epilayer on near-strain-free GaN compliant buffer layer and its applications in hetero-epitaxial LEDs. Scientific Reports, 2015, 5, 13671.	3.3	51
76	Impact of AlO <inf>x</inf> interfacial layer and switching mechanism in W/AlO <inf>x</inf> /TaO <inf>x</inf> /TiN RRAMs. , 2014, , .		2
77	Three phase crystallography and solute distribution analysis during residual austenite decomposition in tempered nanocrystalline bainitic steels. Materials Characterization, 2014, 88, 15-20.	4.4	18
78	Enhanced resistive switching phenomena using low-positive-voltage format and self-compliance IrO x /GdO x /W cross-point memories. Nanoscale Research Letters, 2014, 9, 12.	5.7	30
79	Conductive and transparent multilayer films for low-temperature TiO2/Ag/SiO2 electrodes by E-beam evaporation with IAD. Nanoscale Research Letters, 2014, 9, 35.	5.7	41
80	High energy spinel-structured cathode stabilized by layered materials for advanced lithium-ion batteries. Journal of Power Sources, 2014, 271, 604-613.	7.8	37
81	Superledge Model for Interphase Precipitation During Austenite-to-Ferrite Transformation. Metallurgical and Materials Transactions A: Physical Metallurgy and Materials Science, 2014, 45, 5351-5361.	2.2	22
82	Low current cross-point memory using gadolinium-oxide switching material. , 2014, , .		0
83	NH4F surface modification of Li-rich layered cathode materials. Solid State Ionics, 2014, 264, 36-44.	2.7	35
84	Investigation on optical and electrical properties of ZnO sandwich structure with metal interlayer. Japanese Journal of Applied Physics, 2014, 53, 05FF05.	1.5	4
85	Secondary hardened bainite. Materials Science and Technology, 2014, 30, 1014-1023.	1.6	28
86	Investigation of the Microstructure, Porosity, Adhesion, and Optical Properties of a WO ₃ Film Fabricated Using an E-Beam System With Ion Beam-Assisted Deposition. IEEE Transactions on Magnetics, 2014, 50, 1-4.	2.1	2
87	Stabilization of retained austenite by the two-step intercritical heat treatment and its effect on the toughness of a low alloyed steel. Materials & Design, 2014, 59, 193-198.	5.1	111
88	Stability of retained austenite in multi-phase microstructure during austempering and its effect on the ductility of a low carbon steel. Materials Science & Engineering A: Structural Materials: Properties, Microstructure and Processing, 2014, 603, 69-75.	5.6	100
89	Structure and properties of hot-pressed lead-free (Ba0.85Ca0.15)(Zr0.1Ti0.9)O3 piezoelectric ceramics. RSC Advances, 2013, 3, 20693.	3.6	47
90	Optical and structural studies of dual wavelength InGaN/GaN tunnel-injection light emitting diodes grown by metalorganic chemical vapor deposition. Thin Solid Films, 2013, 529, 269-274.	1.8	13

#	Article	IF	CITATIONS
91	Structural investigation of ZnO:Al films deposited on the Si substrates by radio frequency magnetron sputtering. Thin Solid Films, 2013, 545, 183-187.	1.8	12
92	Structural analysis of Au/TiO2 thin films deposited on the glass substrate. Applied Physics Letters, 2013, 102, .	3.3	12
93	The transition from interphase-precipitated carbides to fibrous carbides in a vanadium-containing medium-carbon steel. Scripta Materialia, 2013, 68, 829-832.	5.2	29
94	Tunable Optical and Structural Properties of Mg <i>_x</i> Zn _{1â^`<i>x</i>} O Films Prepared by In Situ Atomic Layer Doping Technique. ECS Journal of Solid State Science and Technology, 2013, 2, P31-P35.	1.8	2
95	Unipolar Resistive Switching Memory Characteristics Using IrOx/Al2O3/SiO2/p-Si MIS Structure. ECS Transactions, 2012, 45, 345-348.	0.5	2
96	The influence of WidmanstÃ u ten ferrite on yielding behavior of Nb-containing reinforcing steel bars. Scripta Materialia, 2012, 67, 431-434.	5.2	5
97	ZnO-based ultra-violet light emitting diodes and nanostructures fabricated by atomic layer deposition. Semiconductor Science and Technology, 2012, 27, 074005.	2.0	46
98	Formation polarity dependent improved resistive switching memory characteristics using nanoscale (1.3 nm) core-shell IrOx nano-dots. Nanoscale Research Letters, 2012, 7, 194.	5.7	48
99	Twinned formation in weld metal of titanium bearing nano precipitated high strength steel. Materials Chemistry and Physics, 2012, 136, 1103-1108.	4.0	3
100	Blue-shifted stimulated emission from ZnO films deposited on SiO2 by atomic layer deposition. Materials Chemistry and Physics, 2012, 135, 88-93.	4.0	3
101	Interactions between deformation-induced defects and carbides in a vanadium-containing TWIP steel. Scripta Materialia, 2012, 66, 1018-1023.	5.2	89
102	Solution processable nanocarbon platform for polymer solar cells. Energy and Environmental Science, 2011, 4, 3521.	30.8	47
103	Interplay of Three-Dimensional Morphologies and Photocarrier Dynamics of Polymer/TiO2Bulk Heterojunction Solar Cells. Journal of the American Chemical Society, 2011, 133, 11614-11620.	13.7	66
104	Particle Size and Morphology of Iridium Oxide Nanocrystals in Non-Volatile Memory Device. Materials Transactions, 2011, 52, 331-335.	1.2	3
105	Low-alloy duplex, directly quenched transformation-induced plasticity steel. Scripta Materialia, 2011, 65, 604-607.	5.2	32
106	Isothermal treatment influence on nanometer-size carbide precipitation of titanium-bearing low carbon steel. Materials Letters, 2011, 65, 396-399.	2.6	44
107	White-Light Electroluminescence From n-ZnO/p-GaN Heterojunction Light-Emitting Diodes at Reverse Breakdown Bias. IEEE Transactions on Electron Devices, 2011, 58, 3970-3975.	3.0	33
108	Complementary use of transmission electron microscopy and atom probe tomography for the examination of plastic accommodation in nanocrystalline bainitic steels. Acta Materialia, 2011, 59, 6117-6123.	7.9	68

#	Article	lF	CITATIONS
109	Interphase precipitation of nanometer-sized carbides in a titanium–molybdenum-bearing low-carbon steel. Acta Materialia, 2011, 59, 6264-6274.	7.9	254
110	Dynamic strain aging in low cycle fatigue of duplex titanium alloys. Materials Science & Engineering A: Structural Materials: Properties, Microstructure and Processing, 2011, 528, 4381-4389.	5.6	22
111	Microtwin formation in the α phase of duplex titanium alloys affected by strain rate. Materials Science & Engineering A: Structural Materials: Properties, Microstructure and Processing, 2011, 528, 2271-2276.	5.6	18
112	Study on sandwich structure of the transparent conducting oxide films prepared by electron beam evaporation at room temperature. , 2011, , .		1
113	Structural and Photoluminescence Properties of ZnO Films Grown on 6H-SiC Substrates by Low-Temperature Atomic Layer Deposition. Journal of the Electrochemical Society, 2011, 158, H1213.	2.9	2
114	P-Type ZnO:P Films Fabricated by Atomic Layer Deposition and Thermal Processing. Journal of the Electrochemical Society, 2011, 158, H516.	2.9	11
115	Effects of Iridium Oxide Thickness and Post Annealing Temperature on the Size and Density of Core-Shell IrOx-Based Nanocrystals of a Nonvolatile Memory Device. ECS Transactions, 2011, 41, 115-119.	0.5	0
116	STRUCTURAL INVESTIGATION OF n- ZnO /p- GaN ULTRAVIOLET LIGHT-EMITTING DIODES GROWN BY ATOMIC LAYER DEPOSITION. Functional Materials Letters, 2011, 04, 221-224.	1.2	3
117	Temperature-Dependent Physical and Memory Characteristics of Atomic-Layer-Deposited <mml:math xmlns:mml="http://www.w3.org/1998/Math/MathML"><mml:mrow><mml:msub><mml:mrow><mml:mtext>Ru Nanocrystal Capacitors. Journal of Nanomaterials, 2011, 2011, 1-12.</mml:mtext></mml:mrow></mml:msub></mml:mrow></mml:math 	O <b ₂∷nnl:m	tex 6 >
118	Materials science and engineering at National Taiwan University. International Heat Treatment and Surface Engineering, 2010, 4, 48-49.	0.2	0
119	Fabrication of ZnO Nanopillars by Atomic Layer Deposition. Materials Transactions, 2010, 51, 253-255.	1.2	11
120	Structure and Electro-Optical Properties of Thin Films Grown by Alternate Atomic Layer Deposition of ZnO and Al ₂ 0 ₃ on the Sapphire Substrate. Materials Transactions, 2010, 51, 219-226.	1.2	17
121	ZnO-based heterojunction light-emitting diodes on p-SiC(4H) grown by atomic layer deposition. Applied Physics B: Lasers and Optics, 2010, 98, 767-772.	2.2	32
122	Structure and Ultraviolet Electroluminescence of \$n hbox{-ZnO/SiO}_{2}hbox{-ZnO}\$ Nanocomposite/\$p\$ -GaN Heterostructure Light-Emitting Diodes. IEEE Transactions on Electron Devices, 2010, 57, 2195-2202.	3.0	12
123	UV Electroluminescence and Structure of n-ZnO/p-GaN Heterojunction LEDs Grown by Atomic Layer Deposition. IEEE Journal of Quantum Electronics, 2010, 46, 265-271.	1.9	34
124	Inducement of bainite and carbide transformation from retained austenite based on a high strain rate. Scripta Materialia, 2010, 62, 372-375.	5.2	3
125	Substructures of martensite in Fe–1C–17Cr stainless steel. Scripta Materialia, 2010, 62, 670-673.	5.2	27
126	Temperature-dependent photoluminescence of arsenic-doped Si nanocrystals. Journal of Luminescence, 2010, 130, 1485-1488.	3.1	4

#	Article	lF	CITATIONS
127	Structure and stimulated emission of a high-quality zinc oxide epilayer grown by atomic layer deposition on the sapphire substrate. Thin Solid Films, 2010, 519, 536-540.	1.8	19
128	Electron microscopy investigations of V defects in multiple InGaN/GaN quantum wells and InGaN quantum dots. Journal of Microscopy, 2010, 237, 275-281.	1.8	2
129	Density and Grain Size of the IrOx Metal Nanocrystals in n-Si/SiO2/Al2O3/IrOx/Al2O3 Memory Capacitors. ECS Transactions, 2010, 33, 333-337.	0.5	0
130	The Structure and Ultraviolet Electroluminescence of n-ZnO-SiO2-ZnO Nanocomposite/p-GaN Heterojunction LED. ECS Transactions, 2010, 33, 267-275.	0.5	1
131	Characteristics of ALD High-k HfAlOx Nanocrystals in Memory Capacitors Annealed at High Temperatures. ECS Transactions, 2010, 33, 347-353.	0.5	0
132	Stimulated Emission in Highly (0001)-Oriented ZnO Films Grown by Atomic Layer Deposition on the Amorphous Glass Substrates. Journal of the Electrochemical Society, 2010, 157, H879.	2.9	8
133	Amplified Spontaneous Emission From ZnO in n-ZnO/p-GaN Heterojunction Light-Emitting Diodes With an External-Feedback Reflector. IEEE Photonics Technology Letters, 2010, 22, 248-250.	2.5	6
134	Orientation relationship transition of nanometre sized interphase precipitated TiC carbides in Ti bearing steel. Materials Science and Technology, 2010, 26, 421-430.	1.6	73
135	Physical and Memory Characteristics of Atomic-Layer-Deposited High-κ Hafnium–Aluminum-Oxide Nanocrystal Capacitors with Iridium-Oxide Metal Gate. Japanese Journal of Applied Physics, 2009, 48, 05DF02.	1.5	8
136	Characterization of interphase-precipitated nanometer-sized carbides in a Ti–Mo-bearing steel. Scripta Materialia, 2009, 61, 616-619.	5.2	103
137	Simulated heat affected zone in ASTM A533-B steel plates under low heat inputs. Materials Chemistry and Physics, 2009, 117, 471-477.	4.0	11
138	Suppression of phase separation in InGaN layers grown on lattice-matched ZnO substrates. Journal of Crystal Growth, 2009, 311, 4628-4631.	1.5	21
139	The variation of beta phase morphology after creep and negative creep for duplex titanium alloys. Journal of Materials Science, 2009, 44, 408-413.	3.7	4
140	Cross-sectional observation of the intermetallic phase in a galvannealed steel. Materials Science & Engineering A: Structural Materials: Properties, Microstructure and Processing, 2009, 499, 45-48.	5.6	11
141	Precipitation hardening of high-strength low-alloy steels by nanometer-sized carbides. Materials Science & Engineering A: Structural Materials: Properties, Microstructure and Processing, 2009, 499, 162-166.	5.6	202
142	ZnO quantum dots embedded in a SiO ₂ nanoparticle layer grown by atomic layer deposition. Physica Status Solidi - Rapid Research Letters, 2009, 3, 88-90.	2.4	15
143	An efficient Si light-emitting diode based on an n- ZnO/SiO ₂ –Si nanocrystals-SiO ₂ /p-Si heterostructure. Nanotechnology, 2009, 20, 445202.	2.6	15
144	Optical properties and material studies of InGaN/GaN multi-quantum well light emitting diode wafers with different structures. Proceedings of SPIE, 2009, , .	0.8	0

#	Article	IF	CITATIONS
145	Effects of dynamic impact on mechanical properties and microstructure of special stainless steel weldments. Materials Chemistry and Physics, 2008, 111, 172-179.	4.0	8
146	Ultraviolet Electroluminescence From n-ZnO–SiO\$_{2}\$–ZnO Nanocomposite/p-GaN Heterojunction Light-Emitting Diodes at Forward and Reverse Bias. IEEE Photonics Technology Letters, 2008, 20, 1772-1774.	2.5	36
147	A Transmission Electron Microscopy Observation of Dislocations in GaN Grown on (0001) Sapphire by Metal Organic Chemical Vapor Deposition. Japanese Journal of Applied Physics, 2008, 47, 7998.	1.5	12
148	STRUCTURAL AND OPTICAL PROPERTIES OF InGaN / GaN MULTIPLE QUANTUM WELL LIGHT EMITTING DIODES GROWN BY METALORGANIC CHEMICAL VAPOR DEPOSITION. , 2008, , 57-88.		0
149	NANOSTRUCTURAL ANALYSIS OF A GaN-BASED VIOLET LASER DIODE. Surface Review and Letters, 2008, 15, 189-193.	1.1	1
150	Low Voltage Operation of High-κ HfO ₂ /TiO ₂ /Al ₂ O ₃ Single Quantum Well for Nanoscale Flash Memory Device Applications. Japanese Journal of Applied Physics, 2008, 47, 1818.	1.5	10
151	Optical and structural properties of dual wavelength InGaN/GaN multiple quantum well light emitting diodes. , 2008, , .		0
152	Influence of High Indium Composition InGaN on Lattice Matched ZnO Sacrificial Substrates. Journal of Light and Visual Environment, 2008, 32, 143-147.	0.2	1
153	HfO2/HfAlO/HfO2Nanolaminate Charge Trapping Layers for High-Performance Nonvolatile Memory Device Applications. Japanese Journal of Applied Physics, 2007, 46, 1803-1807.	1.5	11
154	Charge storage characteristics of atomic layer deposited RuOx nanocrystals. Applied Physics Letters, 2007, 90, 253108.	3.3	41
155	Observation of ultrahigh density InGaN quantum dots. Journal of Applied Physics, 2007, 102, 013521.	2.5	4
156	Observation of V Defects in Multiple InGaN/GaN Quantum Well Layers. Materials Transactions, 2007, 48, 894-898.	1.2	14
157	Photoluminescence dynamics and structural investigation of InGaN/GaN multiple quantum well light emitting diodes grown by metalorganic chemical vapor deposition. , 2007, , .		0
158	Structural analysis of strained p-type AlGaNâ^•GaN superlattice. Journal of Applied Physics, 2007, 101, 023521.	2.5	7
159	Inverse effect of strain rate on mechanical behavior and phase transformation of superaustenitic stainless steel. Scripta Materialia, 2007, 56, 717-720.	5.2	38
160	Sympathetic nucleation of austenite in a Fe–22Cr–5Ni duplex stainless steel. Scripta Materialia, 2007, 56, 673-676.	5.2	22
161	Cyclic deformation and phase transformation of 6Mo superaustenitic stainless steel. Metals and Materials International, 2007, 13, 275-283.	3.4	22
162	Decomposition of Retained Austenite in a High-Speed Steel GPM A30. Journal of Materials Engineering and Performance, 2007, 16, 102-108.	2.5	1

#	Article	IF	CITATIONS
163	Effect of Retained Austenite on GPM A30 High-Speed Steel. Journal of Materials Engineering and Performance, 2007, 16, 500-507.	2.5	7
164	Cross-sectional transmission electron microscopy of ultra-fine wires of AISI 316L stainless steel. Philosophical Magazine, 2006, 86, 237-251.	1.6	7
165	Gamma (γ) phase transformation in pulsed GTAW weld metal of duplex stainless steel. Materials Science & Engineering A: Structural Materials: Properties, Microstructure and Processing, 2006, 420, 26-33.	5.6	48
166	Martensitic transformations in AISI 440C stainless steel. Materials Science & Engineering A: Structural Materials: Properties, Microstructure and Processing, 2006, 438-440, 276-280.	5.6	17
167	Study of carrier localization in InGaN/GaN quantum well blue-light-emitting diode structures. Journal of Crystal Growth, 2006, 287, 354-358.	1.5	15
168	Nano-structure study of ZnO thin films on sapphire grown with different temperature conditions. Journal of Crystal Growth, 2006, 293, 344-350.	1.5	9
169	Optical and structural properties of InGaN/GaN multiple quantum well structure grown by metalorganic chemical vapor deposition. Thin Solid Films, 2006, 498, 123-127.	1.8	28
170	The effect of strain ratio on morphology of dislocation in low cycle fatigued SAF 2205 DSS. Materials Chemistry and Physics, 2006, 98, 103-110.	4.0	19
171	Study of InGaN Multiple Quantum Dots by Metal Organic Chemical Vapor Deposition. Japanese Journal of Applied Physics, 2006, 45, 3560-3563.	1.5	4
172	Mechanical stabilisation of austenite. Materials Science and Technology, 2006, 22, 641-644.	1.6	194
173	Structure and formation mechanism of V defects in multiple InGaNâ^•GaN quantum well layers. Journal of Applied Physics, 2006, 99, 073505.	2.5	124
174	Structural and compositional analyses of a strained AlGaNâ^•GaN superlattice. Journal of Applied Physics, 2006, 100, 013110.	2.5	15
175	Metalorganic chemical vapor deposition and structural/optical characteristics of InGaN/GaN multiple quantum wells grown on sapphire for light emitting diode application. , 2005, , .		Ο
176	Effects of silicon doping on the nanostructures of InGaN/GaN quantum wells. Journal of Crystal Growth, 2005, 279, 55-64.	1.5	14
177	Low-cycle fatigue-induced martensitic transformation in SAF 2205 duplex stainless steel. Materials Science & Engineering A: Structural Materials: Properties, Microstructure and Processing, 2005, 398, 349-359.	5.6	40
178	Characterisation of severely deformed austenitic stainless steel wire. Materials Science and Technology, 2005, 21, 1323-1328.	1.6	39
179	Determination of thickness and lattice distortion for the individual layer of strained Al0.14Ga0.86Nâ^•GaN superlattice by high-angle annular dark-field scanning transmission electron microscopy. Applied Physics Letters, 2005, 87, 031914.	3.3	8
180	Nanostructures and carrier localization behaviors of green-luminescence InGaN/GaN quantum-well structures of various silicon-doping conditions. Applied Physics Letters, 2004, 84, 2506-2508.	3.3	59

#	Article	IF	CITATIONS
181	Improvements of InGaNâ^•GaN quantum-well interfaces and radiative efficiency with InN interfacial layers. Applied Physics Letters, 2004, 84, 5422-5424.	3.3	16
182	High-Resolution Scanning Electron Microscopy Observation of GaN/AlGaN Strained-Layer Superstructures in GaN-Based Violet Laser Diodes. Japanese Journal of Applied Physics, 2004, 43, 968-969.	1.5	6
183	The low-temperature aging embrittlement in a 2205 duplex stainless steel. Materials Science & Engineering A: Structural Materials: Properties, Microstructure and Processing, 2004, 379, 119-132.	5.6	141
184	Mapping of multiple-quantum-well layers and structure of V defects in InGaN/GaN diodes. Applied Physics Letters, 2004, 84, 2271-2273.	3.3	12
185	Title is missing!. Journal of Materials Science, 2003, 38, 2373-2391.	3.7	10
186	Microstructural degeneration of simulated heat-affected zone in 2.25Cr–1Mo steel during high-temperature exposure. Materials Science & Engineering A: Structural Materials: Properties, Microstructure and Processing, 2003, 340, 15-32.	5.6	18
187	Formation and structure of inverted hexagonal pyramid defects in multiple quantum wells InGaN/GaN. Applied Physics Letters, 2003, 82, 718-720.	3.3	66
188	Atomic-scale strain field and In atom distribution in multiple quantum wells InGaN/GaN. Applied Physics Letters, 2003, 82, 715-717.	3.3	48
189	Direct determination of atomic structure in multiple quantum wells InGaN/GaN. Applied Physics Letters, 2002, 80, 761-762.	3.3	22
190	Aging reactions in a 17-4 PH stainless steel. Materials Chemistry and Physics, 2002, 74, 134-142.	4.0	317
191	Phase transformation in AISI 410 stainless steel. Materials Science & Engineering A: Structural Materials: Properties, Microstructure and Processing, 2002, 332, 1-10.	5.6	92
192	Microstructural characterization of simulated heat affected zone in a nitrogen-containing 2205 duplex stainless steel. Materials Science & Engineering A: Structural Materials: Properties, Microstructure and Processing, 2002, 338, 166-181.	5.6	104
193	The effect of high-temperature exposure on the microstructural stability and toughness property in a 2205 duplex stainless steel. Materials Science & Engineering A: Structural Materials: Properties, Microstructure and Processing, 2002, 338, 259-270.	5.6	292
194	Effects of solution treatment and continuous cooling on σ-phase precipitation in a 2205 duplex stainless steel. Materials Science & Engineering A: Structural Materials: Properties, Microstructure and Processing, 2001, 311, 28-41.	5.6	254
195	The effect of prior compressive deformation of austenite on toughness property in an ultra-low carbon bainitic steel. Materials Chemistry and Physics, 2001, 69, 113-124.	4.0	41
196	Growth of highly transparent nanocrystalline diamond films and a spectroscopic study of the growth. Journal of Applied Physics, 2001, 89, 753-759.	2.5	43
197	Age Hardening in Martensitic/Bainitic Matrices in a Copper-Bearing Steel. Materials Transactions, JIM, 2000, 41, 1312-1321.	0.9	10
198	The effect of compressive deformation of austenite on the bainitic ferrite transformation in Feî—,Mnî—,Siî—,C steels. Materials Science & Engineering A: Structural Materials: Properties, Microstructure and Processing, 2000, 278, 278-291.	5.6	68

#	Article	IF	CITATIONS
199	Growth, characterization, optical and X-ray absorption studies of nano-crystalline diamond films. Diamond and Related Materials, 2000, 9, 877-882.	3.9	25
200	The effect of compressive deformation of austenite on the Widmanstäten ferrite transformation in Fe–Mn–Si–C steel. Materials Science & Engineering A: Structural Materials: Properties, Microstructure and Processing, 1999, 264, 139-150.	5.6	20
201	Microstructures and fatigue crack growth of EH36 TMCP steel weldments. International Journal of Fatigue, 1999, 21, 857-864.	5.7	49
202	Quantum Confinement Effect in Diamond Nanocrystals Studied by X-Ray-Absorption Spectroscopy. Physical Review Letters, 1999, 82, 5377-5380.	7.8	118
203	Microstructures of Heat-Affected Zone in Niobium Containing Steels. Materials Transactions, JIM, 1999, 40, 199-208.	0.9	6
204	Highly transparent nano-crystalline diamond films via substrate pretreatment and methane fraction optimization. Thin Solid Films, 1998, 332, 34-39.	1.8	30
205	Highly transparent nano-crystalline diamond films grown by microwave CVD. Solid State Communications, 1998, 107, 301-305.	1.9	15
206	Effects of substrate pretreatment and methane fraction on the optical transparency of nanocrystalline diamond thin films. Journal of Materials Research, 1998, 13, 1769-1773.	2.6	22
207	Microstructural evolution of simulated heat affected zone in ASTM A533 type B steel plates. Science and Technology of Welding and Joining, 1997, 2, 119-127.	3.1	4
208	The effect of stress on the Widmanstäten ferrite transformation. Materials Science & Engineering A: Structural Materials: Properties, Microstructure and Processing, 1997, 223, 158-167.	5.6	24
209	Mechanical Stabilization of Austenite against Bainitic Reaction in Fe–Mn–Si–C Bainitic Steel. Materials Transactions, JIM, 1996, 37, 579-585.	0.9	44
210	The Influence of Plastic Deformation and Cooling Rates on the Microstructural Constituents of an Ultra-low Carbon Bainitic Steel ISIJ International, 1995, 35, 1013-1019.	1.4	26
211	Acicular ferrite transformation in deformed austenite of an alloy-steel weld metal. Journal of Materials Science, 1995, 30, 5036-5041.	3.7	7
212	Influence of acicular ferrite and bainite microstructures on toughness for an ultra-low-carbon alloy steel weld metal. Journal of Materials Science Letters, 1993, 12, 1290-1293.	0.5	36
213	Formation of austenite from a mixture of bainitic ferrite and austenite. Materials Chemistry and Physics, 1993, 35, 168-175.	4.0	3
214	Microstructural examination of 2.25Crî—,1Mo Steel Steam pipes after extended service. Materials Characterization, 1993, 30, 75-88.	4.4	31
215	Microstructural and electrical properties of epitaxial PtSi/pâ€Si(100) coâ€deposited under ultrahigh vacuum. Journal of Applied Physics, 1993, 74, 6251-6255.	2.5	13
216	Effect of Compressive Deformation on the Transformation Behavior of an Ultra-Low-Carbon Bainitic Steel. Materials Transactions, JIM, 1993, 34, 658-668.	0.9	29

#	Article	IF	CITATIONS
217	The coexistence of acicular ferrite and bainite in an alloy-steel weld metal. Journal of Materials Science Letters, 1992, 11, 1145-1146.	0.5	5
218	Effects of chemical composition, rolling and cooling conditions on the amount of martensite/austenite (M/A) constituent formation in low carbon bainitic steels. Materials Science & Engineering A: Structural Materials: Properties, Microstructure and Processing, 1992, 154, 43-49.	5.6	50
219	The development of ultra-low-carbon bainitic steels. Materials & Design, 1992, 13, 335-338.	5.1	26
220	The effects of rolling processes on the microstructure and mechanical properties of ultralow carbon bainitic steels. Materials Science & Engineering A: Structural Materials: Properties, Microstructure and Processing, 1992, 157, 29-36.	5.6	24
221	Continuous heating transformation of bainite to austenite. Materials Science & Engineering A: Structural Materials: Properties, Microstructure and Processing, 1991, 131, 99-113.	5.6	36
222	Acicular ferrite transformation in alloy-steel weld metals. Journal of Materials Science, 1991, 26, 839-845.	3.7	44
223	Dual ferrite-martensite treatments of a high-strength low-alloy ASTM A588 steel. Journal of Materials Science, 1991, 26, 889-898.	3.7	11
224	Reaustenitization experiments on some high-strength steel weld deposits. Materials Science & Engineering A: Structural Materials: Properties, Microstructure and Processing, 1989, 118, 155-170.	5.6	16
225	Orientation relationships between adjacent plates of acicular ferrite in steel weld deposits. Materials Science and Technology, 1989, 5, 93-97.	1.6	52